Calmodulin-induced conformational and hydrodynamic changes in the catalytic domain of Bordetella pertussis adenylate cyclase toxin.

Johanna C Karst, Ana Cristina Sotomayor Pérez, J Iñaki Guijarro, Bertrand Raynal, Alexandre Chenal, Daniel Ladant

Calmodulin-Induced Conformational and Hydrodynamic Changes of the Catalytic Domain of *Bordetella pertussis* Adenylate Cyclase Toxin †

Johanna C. Karst‡, Ana Cristina Sotomayor Pérez‡, J. Iñaki Guijarro§, Bertrand Raynal‖, Alexandre Chenal‡*⊥, and Daniel Ladant‡*⊥

‡ Institut Pasteur, Unité de Biochimie des Interactions Macromoléculaires, CNRS URA 2185, Département de Biologie Structurale et Chimie, 25-28 rue du Dr. Roux, 75724 Paris Cedex 15, France

§ Institut Pasteur, Unité de RMN des Biomolécules, CNRS URA 2185, Département de Biologie Structurale et Chimie, 25-28 rue du Dr. Roux, 75724 Paris Cedex 15, France

‖ Institut Pasteur, Plate-Forme de Biophysique des Macromolécules et de leurs Interactions, CNRS URA 2185, Département de Biologie Structurale et Chimie, 25-28 rue du Dr. Roux, 75724 Paris Cedex 15, France.

* To whom correspondence should be addressed: Daniel Ladant, Unité de Biochimie des Interactions Macromoléculaires, CNRS URA 2185, Institut Pasteur, 28 rue du Dr. Roux, 75724 Paris cedex 15, France. Tel: 331 45 68 84 00; Fax: 331 40 61 30 42; email: daniel.ladant@pasteur.fr; or Alexandre Chenal, Unité de Biochimie des Interactions Macromoléculaires, CNRS URA 2185, Institut Pasteur, 28 rue du Dr. Roux, 75724 Paris cedex 15, France. Tel: 331 44 38 92 12; Fax: 331 40 61 30 42; email: alexandre.chenal@pasteur.fr

⊥ These authors contributed equally to this work.

Running title: Calmodulin-induced changes of the catalytic domain of *CyaA*

Abbreviations

AC, adenylate cyclase domain; CyaA, adenylate cyclase toxin; CaM, calmodulin; EF, Edema

factor; HEPES, (N-[2-hydroxyethyl]piperazine-N'-[2-ethanesulfonic acid]); λmax, maximum

emission wavelength; CD, circular dichroism; MRE, mean residue ellipticity; AUC, analytical

ultracentrifugation; SEC-TDA, size exclusion chromatography coupled on-line to a Triple

Detector Array; QELS, Quasi-elastic light scattering; SDS-PAGE, sodium dodecyl sulfate-

polyacrylamide gel electrophoresis; R_H, hydrodynamic radius; R_0, anhydrous hydrodynamic

radius.

Abstract

Bordetella pertussis, the causative agent of whooping cough, secretes among various toxins an adenylate cyclase (CyaA) that displays a unique mechanism of cell invasion, which involves a direct translocation of its N-terminal catalytic domain (AC, 400 residues) across the plasma membrane of the eukaryotic targeted cells. Once into the cytosol, AC is activated by endogenous calmodulin and produces toxic amounts of cAMP. The structure of AC in complex with the C-terminal part of calmodulin has been recently solved. However, as the structure of the catalytic domain in the absence of calmodulin is still lacking, the molecular basis of AC activation by calmodulin remains largely unknown. To characterize this activation mechanism, we investigated here the biophysical properties of the isolated catalytic domain in solution with or without calmodulin. We found that calmodulin triggered only minor modifications of the protein secondary and tertiary structure but had pronounced effect on the hydrodynamic properties of AC. Indeed, while the isolated catalytic domain was spherical and hydrated, it underwent a significant elongation as well as compaction and dehydration upon calmodulin interaction. Based on these data, we propose a model for the structural transition between the calmodulin-free and calmodulin-bound AC.

The adenylate cyclase toxin (CyaA) produced by *Bordetella pertussis*, the causative agent of whooping cough, is a key virulence factor of this bacterium (*1, 2*). It is secreted by virulent bacteria, and is able to invade eukaryotic cells where, upon activation by the endogenous calmodulin (CaM), it catalyzes unregulated synthesis of cAMP up to pathogenic levels. The CyaA toxin plays an important role in the early stages of respiratory tract colonization by *B. pertussis*. Through its interaction with a cellular receptor, the CD11b/CD18 integrin, CyaA targets cells from the innate immune system (i.e. neutrophils, macrophages, etc.) and impairs their phagocytic functions (*3-5*). CyaA is a 1706 residue-long protein: the CaM-activated catalytic domain (AC) is located in the 400 amino-proximal residues while the carboxy-terminal 1306 residues constitute the major calcium-binding region (*6-8*) and are responsible for binding to target cells and translocation of the N-terminal catalytic domain across the cell plasma membrane by a yet undisclosed mechanism. The AC domain interacts with high affinity (K_D < 0.1 nM) with CaM to form a complex that exhibits a very high catalytic turnover (k_{cat} = 2,000 - 3,000 s^{-1}), while the enzymatic activity of AC alone is about 1000-fold lower.

CyaA belongs to a subclass of adenylate cyclase enzymes that comprises different toxins secreted by pathogenic bacteria (*9, 10*). Among them, the closest relative to CyaA and most studied member of this sub-family is the Edema Factor (EF) of *Bacillus anthracis*, a toxin crucial for anthrax pathogenesis. The EF toxin associated with the *B. anthracis* protective antigen (PA) uses a receptor-mediated endocytosis pathway to enter eukaryotic cells, where it is, like CyaA, activated by CaM to produce supraphysiologic levels of cAMP.

Although AC and EF exhibit only limited sequence identity (*10*), they share substantial similarity in their tertiary structures as revealed by the X-ray structures of both enzymes in

complex with CaM (*10, 11*). Most interestingly, although the respective CaM contact surfaces in the two enzymes have largely diverged, their catalytic sites, made of three highly conserved regions (CR1, residues 54-77; CR2, residues 184-198; CR3, residues 295-315), are structurally identical. Prior mutagenesis studies have shown that many of the conserved residues in these segments play a direct role in the catalytic reaction (*12-14*). A detailed structural comparison of EF alone or as a complex with CaM, revealed that one of the conserved region (CR3) lining the active site is disordered in the absence of CaM. This study demonstrated a novel mechanism of CaM-mediated activation by active site remodeling (*15*). However, the molecular basis of CaM activation of AC remains unknown, as the structure of the isolated CyaA catalytic domain is lacking.

Prior biochemical studies have shown that the AC domain has a modular structure: it consists of two regions, T25 (residues 1-224 of CyaA) and T18 (residues 225-384) that can be obtained *in vitro* by limited proteolysis (*16*). The isolated T25 and T18 fragments can re-associate with CaM into a fully active ternary complex (*17, 18*). The crystal structure of the CyaA catalytic domain bound to the C-terminal domain of CaM (CaM_{C-ter}) showed that the complex has an elongated shape and that CaM_{C-ter} interacts predominantly with the C-terminal, T18 moiety of AC (*11, 16, 19, 20*). In particular, an amphiphilic helical structure (residues 234-254), defined as helix H by Guo *et al.* (*11*) was found to be a major determinant of CaM binding.

Here, in an attempt to understand how CaM might activate CyaA, we have characterized by complementary biophysical approaches, the conformational and hydrodynamic changes of AC induced by CaM-binding. We found that CaM binding triggered only limited modifications of the secondary and tertiary structures of AC but induced drastic changes of its

hydrodynamic properties: while the isolated catalytic domain was spherical and hydrated, CaM interaction elicited significant elongation and dehydration of the complex. The implications of these findings for the mechanism of AC activation by CaM are discussed.

Experimental Procedures

Materials

Hepes-d18 (D18, 98%, DLM-3786-0) was purchased from Cambridge Isotope Laboratories. D_2O (D215B), NaOD and DCl were from Euriso-top (C.E.A. Saclay, Gif-Sur-Yvette, France). All experiments were done in 20 mM Hepes, 150 mM NaCl, pH 7.4, (buffer A) supplemented or not with 0.2 mM $CaCl_2$ at 25 °C. The peptide $P_{233-254}$ was synthesized and purified by Genosphere Biotechnologies (Paris, France). Its sequence is LDRERIDLLWKIARAGARSAVG and corresponds to the amino-acid sequence between residues 233 and 254 (native numbering) of CyaA. The peptide contains 22 amino-acids, 1 native tryptophan and is N-acetylated. It was purified to homogeneity by reversed-phase HPLC on a C8 column using an acetonitrile/trifluoroacetic acid gradient. Its quality was assessed by Matrix Assisted Laser Desorption Ionisation - Time Of Flight (MALDI-TOF). Its molecular mass determined by MALDI-TOF is 2509 Da and its pK is computed to be 10.7.

Protein preparation

The adenylate cyclase catalytic domain (AC) studied here corresponds to residues 1 to 384 of *Bordetella pertussis* CyaA followed by a glycine and a lysine residues (*21*). AC was overproduced in *Escherichia coli* and purified by two sequential chromatographic steps on DEAE-sepharose as described by Vougier *et al.* (*21*). The elution buffer of the DEAE-

sepharose was 20 mM Hepes, 500 mM NaCl, pH 7.4. AC was further purified on a sephacryl S300 column equilibrated with buffer A. Purified AC was equilibrated in buffer A or in 20 mM NH_4HCO_3 by chromatography on prepacked G25SF desalting columns prior to lyophilization. The protein, in solution or lyophilized, was stored at –20 °C. We checked by CD and fluorescence that the lyophilization process did not affect the behavior of AC. Protein batches were homogeneous as analyzed by SDS-PAGE and N-terminal sequencing. The integrity and identity of the samples were confirmed by the measurement of the absolute molecular mass by surface enhanced laser desorption/ionization time-of-flight mass spectrometry (SELDI-TOF-MS model PCS 4000, Ciphergen). The mass spectrum showed a single peak of 41580 +/- 300 $g.mol^{-1}$, which corresponded to the expected molecular weight (41588 $g.mol^{-1}$). A molar epsilon of 28880 $M^{-1}.cm^{-1}$ and a pI of 6.3 were computed from the sequence of AC.

The thermodynamic stability of AC was investigated by tryptophan fluorescence and circular dichroism. The data showed that AC was weakly stable (half-melting temperature of 41°C) and prone to aggregation in a temperature dependant-manner. We also checked that fluorescence, far-UV and near-UV CD spectra of AC were not sensitive to calcium (from 0 to 2 mM $CaCl_2$). We thus chose to perform all experiments at 25 °C and in the presence of 0.2 mM calcium (required for full-saturation of CaM).

The purified AC protein exhibited a specific enzymatic activity of 2 – 4 units/mg in the absence of calmodulin (CaM) and about 2000 units/mg in the presence of 2 nM CaM; it was half-maximally activated by a CaM concentration of about 0.1 nM. One unit of AC enzymatic activity, measured as described previously (*16*), corresponds to 1 μmol of cAMP formed per minute at 30 °C and pH 8.

CaM was overproduced in *E. coli* and purified as described by Vougier *et al*. (*21*). A first step of ammonium sulfate precipitation followed by a glacial acetic acid precipitation and a

phenyl-sepharose chromatography leaded to a protein, which was more than 95% pure as judged by SDS-PAGE. As performed for AC, N-terminal sequencing and mass spectrometry confirmed the integrity and identity of CaM. The mass spectrum showed a single peak of 16710 +/- 100 g.mol^{-1}, which was in agreement with the expected molecular weight (16709 g.mol^{-1} after removal of the N-terminal methionine). A molar epsilon of 2980 M^{-1}.cm^{-1} and a pI of 4.1 were computed from the sequence of CaM.

Circular dichroism spectroscopy

CD spectra were recorded on an Aviv circular dichroism spectrometer model 215, equipped with a water-cooled Peltier unit. CD measurements were carried out at a scan rate of 0.5 nm/sec (step: 0.5 nm and integration time: 1 sec) with a time constant of 100 msec and a bandwidth of 1 nm. Each far-UV and near-UV CD spectrum represents the average of at least 5 scans. Buffer A supplemented with 0.2 mM calcium was used as blank in the far-UV and near-UV regions and its spectra was subtracted from all recorded CD spectra.

Far-UV CD spectra were recorded in rectangular quartz Suprasil cells of 0.1 mm path lengths (106.QS, Hellma) with 25 μM protein (AC, CaM, AC/CaM or peptide/CaM 1:1 mixture) or 90 μM for the free peptide in buffer A supplemented with 0.2 mM CaCl$_2$. The CD unit used is the mean residue ellipticity $[\theta]_F$ (MRE) expressed in degrees square centimeter per decimole residue ((deg*cm^2)/(dmol*res)) and calculated as previously described (*8*).

Measured ellipticity in mdeg obtained for individual AC (386 residues) and CaM (148 residues) spectra were added and converted to mean residue ellipticity taking into account the total number of residues present in a complex in a 1:1 stoichiometry, i.e. 534 residues. The resulting spectrum was compared to the spectrum of the AC/CaM sample. A similar analysis was performed with the peptide P$_{233-254}$ (22 residues).

Near-UV CD measurements were performed by using a tandem cuvette (238.QS, Hellma).

Proteins were placed in separated chambers and then mixed in the same cuvette without removing the sample, thereby maintaining identical contents before and after mixing. AC at 30 μM (or peptide at 45 μM) and CaM at 30 μM in buffer A supplemented with 0.2 mM $CaCl_2$ were placed into separate chambers of the tandem cuvette and spectra were acquired at 25 °C. Proteins in the two chambers were then mixed by inversion of the cuvette and spectra were recorded in the conditions described above. The CD unit used is the molar ellipticity $[\theta]_N$, expressed in degrees square centimeter per decimole ((deg*cm^2)/dmol) and calculated as previously described (*8*).

Spectra in the far-UV region were deconvoluted using five algorithms (*22-24*) available at the DICHROWEB server: Contin-LL, Selcon 3, CDSSTR, VARSLC and K2d. Here, only the results obtained with the CDSSTR program from W. C. Johnson (*25-27*) are reported as they provided the best fits to all data.

Fluorescence spectroscopy

Measurements were performed with an FP-6200 spectrofluorimeter (Jasco, Japan) in a Peltier-thermostated cell holder, using a 1 cm path length quartz cell (101.QS, Hellma). A bandwidth of 5 nm was used for the excitation and emission beams. Peptide concentration was 1μM in buffer A supplemented with 0.2 mM $CaCl_2$. Calmodulin was progressively added in the cuvette that contained the peptide (in concentrations ranging from 0 to 10 μM final). For tryptophan intrinsic fluorescence, the excitation wavelength was fixed at 290 nm. The emission spectra were recorded at 25 °C, from 300 to 400 nm at a scan rate of 125 nm.min^{-1}. The maximum emission wavelength (λ_{max}) and fluorescence intensity ratio at 360 nm over 320 nm (FIR 360/320) represent the average of three values obtained from emission spectra that were corrected for blank measurements.

Nuclear magnetic resonance spectroscopy (NMR)

NMR experiments were acquired on an Inova (Varian Inc., Palo Alto) spectrometer with a 14.7 Tesla magnetic field (600 MHz proton resonance frequency) equipped with a cryoprobe. The software VnmrJ 2.1B (Varian) was used to record and process data. Proteins were desalted against 10 mM NH_4HCO_3 on G25SF and then lyophilized. Buffer A prepared with deuterated Hepes (d18, Cambridge Isotope Laboratories) and D_2O (99,99%) was lyophilized twice and resuspended in D_2O to remove residual H_2O. The lyophilized proteins were resuspended in a given volume of this buffer, incubated one hour at room temperature to exchange amide protons, and freeze-dried. Proteins were then resuspended in the same volume of D_2O used prior to lyophilization. One-dimensional (1D) ^1H spectra were acquired at 25 °C with AC (40 μM), CAM (50 μM) and AC/CAM (30 μM, 1:1 mixture) in deuterated buffer A. The buffer was supplemented with 2 mM $CaCl_2$ for AC and AC/CAM samples. Sixty-four transients with a spectral width of 12 ppm were accumulated. Water signal was suppressed by very low-power irradiation (0.5 s) during the 2 s recovery delay.

Saturation transfer experiments between aromatic and aliphatic protons were performed by selectively saturating a bandwidth of 1.5 ppm of the aromatic region centred at 7.2 ppm in the saturation experiment or off-resonance at 15 ppm in the reference experiment. Selective saturation was achieved using trains of 90° gaussian pulses. Experiments were run with 24 accumulations for each saturation time that varied between 0 and 2.2 s. The transferred saturation or nOe (nuclear Overhauser enhancement) was calculated using the formula $nOe = | [I_S − I_R] / I_R |$, where I_S and I_R represent the intensities of the aliphatic region (upfield of 1.1 ppm) of the on- and off-resonance experiments, respectively. Build-up curves (nOe versus saturation time t) were fit using an isolated spin-pair relaxation model ($nOe = σ/ρ [1 − exp[-ρt]]$), where $σ$ (s^{-1}) represents the cross-relaxation rate and $ρ$ (s^{-1}) the auto-relaxation rate).

Analytical ultracentrifugation

Sedimentation equilibrium and velocity experiments were performed on a Beckman XL-A analytical ultracentrifuge (Beckman Coulter) in an AN60-Ti rotor at 25 °C. The samples were filtrated on 0.2 μm filters before experiments. Detection of the protein concentration as a function of radial position and time was performed by optical density measurements at a wavelength of 276 nm and 230 nm. The buffer was buffer A supplemented with 0.2 mM CaCl$_2$. The computed viscosity η_s and density ρ of this buffer were (SEDNTERP 1.09) 0.908 cP and 1.004 g.mL^{-1} at 25°C, respectively. For sedimentation equilibrium experiments, the CaM sample (120 μL, 50 μM) was loaded in a 1.2 mm-thick two channels epon centerpiece. It was centrifuged for 24 hours at a rotor speed of 25,000 rpm, then for 15 hrs at 30,000 rpm and finally for 10 hrs at 35,000 rpm. The AC sample (40 μL, 19 μM) was loaded in a 1.2 mm-thick six channels epon centerpiece and was then centrifuged for 3 hours at a rotor speed of 12,000 rpm, for 2 hrs at 15,000 rpm, and for 2 hrs at 18,000 rpm. Finally, the AC/CaM complex sample (150 μL, 17 μM for both protein) was loaded in a 1.2 mm-thick two channels aluminium centerpiece. The complex was centrifuged for 10 hours at a rotor speed of 12,000 rpm, then for 7 hrs at 15,000 rpm and finally for 7 hrs at 18,000 rpm. Data were recorded for each speed after controlling that sedimentation/diffusion equilibrium had been effectively reached. Baseline was measured at 42,000 rpm after 2 hrs for CaM and 50,000 rpm for AC and the complex. Radial distributions were analyzed by global fitting of the 3 speeds using the 1 species model in the Ultrascan 9.5 software (*28*). Partial specific volume was obtained by fixing the molecular mass to the mass of the monomer determined by mass spectrometry.

For sedimentation velocity experiments, the protein samples (400 μL, 17 μM) were loaded in a 1.2 mm-thick two channels aluminium centerpiece and spun at 60,000 rpm for CaM or 50,000 rpm for AC and the complex. Data were analyzed with the Sedfit 11.3 software (*29*) using a continuous size distribution c(s) model with a level of confidence of 0.95. Monte

Carlo analysis (1000 iterations) were done for each plot with the Sedfit software (*30*). The errors were below 0.05 % showing the robustness of the fits. The three species, AC, CaM, and the AC/CaM complex, were analyzed by sedimentation velocity experiments at three additional concentrations (8 μM, 14 μM, 27 μM), yielding similar profiles. The hydrodynamic radius, R_H, was calculated using the sedimentation coefficient value and the molecular mass determined by size exclusion chromatography coupled on-line to TDA.

Size exclusion chromatography coupled on-line to hydrodynamic measurements

Size exclusion chromatography (SEC) was carried out on a Superdex 200 column (GE Healthcare). It was controlled by a GPCmax module connected on-line to a triple detector array (TDA) model 302 (Viscotek Ltd., Houston, Basingstoke, U.K.). The oven of the TDA contained (i) a static light scattering cell with two photodiode detectors, at 7° for low angle (LALS) and at 90° for right angle laser light scattering (RALS), (*ii*) a deflection refractometer, (*iii*) a photometer and (*iv*) a differential viscometer. The general procedures are described elsewhere (*8*). Briefly, all solutions were filtered on 0.2 μm filters and allowed to equilibrate at 25 °C prior to running. Buffer A supplemented with 0.2 mM $CaCl_2$ was used and the SEC experiments were performed at 22 °C. The detections in the TDA oven were done at 25 °C. All experimental sequences contained injections of BSA used for TDA calibration (2 mg/mL, various volumes) and at least four injections of different volumes of the tested protein (i.e. AC 20 μM, CaM 40 μM, and AC/CaM complex 17 μM for both proteins). The refractive index increments, dn/dc, were experimentally determined. All data were acquired and processed using the Omnisec software (Viscotek Ltd.). Protein concentration was determined using both the photometer and the deflection refractometer. The RALS and LALS data coupled to the concentration provided the molecular mass. Finally, the differential viscometer measurements, in conjunction with concentration, provided the intrinsic viscosity.

Protein shape and hydration

The viscosity increment v (the Simha-Einstein hydrodynamic function related to the axial ratio a/b) of proteins can be calculated by inverting the Einstein's viscosity relation: $M[\eta] = vV_HN_A$ to $v = (M[\eta])/(V_HN_A)$ where V_H is the hydrodynamic volume defined by $V_H = 4\pi R_H^3/3$, $[\eta]$ is the intrinsic viscosity and N_A is the Avogadro number. The R_H values are calculated from the sedimentation coefficient and molecular mass (see above). Hydration δ_{IV} is calculated from the intrinsic viscosity measurement. The intrinsic viscosity in a defined solvent depends on the shape, the molecular volume of the protein and electroviscous effects. Its expression is the product of the hydrodynamic function v and the swollen volume V_s according to: $[\eta] = vV_s = v(\bar{v} + \delta_{IV}/\rho)$, where the swollen volume is given by the sum of the partial specific volume $\bar{v}$ of the protein (volume occupied by one gram of protein) and the hydration of the protein (mass water per mass protein g/g). The hydration parameter δ_{IV} of the protein, which can be extracted from the latter relation: $\delta_{IV} = ((\left[\eta\right]/v) - \bar{v})\rho$, includes (*i*) the water molecules bound to the protein and (*ii*) the water molecules dragged by the diffusion of the protein and/or influenced by being in the vicinity of the protein. The molecular mass M was measured by static light scattering, the partial specific volume $\bar{v}$ by equilibrium AUC and the R_H by velocity AUC (see above). The viscosity increment provides the axial ratio a/b of the semi axes a and b (with a > b) that describe the shape of an ellipsoid of revolution. All theses procedures are described elsewhere (*8, 31*).

Results

Conformational studies of AC and CaM in solution followed by circular dichroism and fluorescence spectroscopies

Modifications of the secondary and tertiary structure contents of the AC polypeptide upon CaM binding were characterized by circular dichroism (CD) spectroscopy. The far-UV CD spectrum of CaM was characteristic of an α-helical protein with minima at 208 and 222 nm (figure 1A). The secondary structure content was estimated by deconvolution procedures using DICHROWEB [(*22-27*); see Experimental procedures and table 1]. The secondary structure content was in good agreement with that deduced from the NMR solution structure of calmodulin (*32*). The far-UV CD spectrum of AC appeared rather unusual with a positive π_0-π* band around 190 nm, a negative π_0-π* band at 207 nm and a weak negative n'-π* band, appearing as a shoulder around 220 nm (figure 1A). The band located at 207 nm may be assigned to a combination of the negative π_0-π* band of extended conformation arising at 200 nm and the negative contribution of the exciton splitting of the π_0-π* band of α-helices at 210 nm. The secondary structure content of AC deduced from this CD spectrum was estimated to be ≈ 24 % of α-helices and ≈ 19 % of β-sheets (table 1). The spectrum of the AC/CaM complex at an equimolar ratio was quite similar (figure 1A), also displaying a negative π_0-π* band around 207 nm and a negative n'-π* band around 220 nm. Upon deconvolution of this CD spectrum, the overall secondary structure composition of the AC/CaM complex (≈ 35 % of α-helices and ≈ 13 % of β-sheets, table 1) turned out to be significantly different from that deduced from the X-ray structure of the AC/CaM$_{C-ter}$ complex which showed a higher proportion of helical structures (≈ 45 % according to the pdb file 1YRU) (*11*). Although secondary structure predictions from CD spectra may sometimes be relatively inaccurate, the variation in α-helical content found could also result from the differences in the AC and CaM

polypeptides examined in each case: our AC protein encompasses residues 1 to 386 and a full-length CaM molecule while the X-ray structure was solved with a crystal made of a complex of AC residues 1-364 bound to only the C-terminal half of CaM (*11*). Finally, aromatic residues of AC might also affect the far-UV CD spectrum, thus altering the secondary structure content deconvolution (*33-35*). Yet it should be stressed that the AC/CaM complex characterized here was fully functional from an enzymatic point of view, exhibiting a high catalytic turnover (k_{cat} = 2,000 - 3,000 s^{-1}) and behaved as a homogenous species according to its hydrodynamic properties (see below). Thus the CD spectral properties reported here likely reflect the intrinsic structural characteristics of the active AC-CaM complex in solution.

To characterize the conformational changes that resulted from CaM binding to AC, we compared the experimental spectrum of the AC-CaM complex (figure 1B, thick line) with the sum (thin line) of the spectra of the two individual proteins at equimolar concentrations (see Experimental Section). As shown in figure 1B, the spectra revealed a significant increase in absolute values in ellipticity of the AC-CaM complex as compared to that of the 2 separated proteins. Interestingly, the difference spectrum (i.e. AC/CaM – (AC + CaM), at equimolar concentrations), as shown in the inset of figure 1B, displayed 2 major bands at 223 nm and 208 nm, suggesting that the formation of the AC/CaM complex is accompanied by an increase in the α-helical content of the polypeptides. Assuming that a signal of -30 Kdeg.cm^2.dmol^{-1} at 223 nm corresponds to $\approx$ 100% of alpha-helical content (*36*), the variation of the ellipticity of about -1.1 $\pm$ 0.3 Kdeg.cm^2.dmol^{-1} should correspond to an increment of about 3.7 $\pm$ 1 % in α-helical content. This corresponds to about 20 $\pm$ 5 amino acids out of a total of 534 residues (386 AC residues plus 148 CaM residues) acquiring an α-helical structure upon interaction of the 2 polypeptides. It is likely that this increase in α-helical

content involved mainly the AC polypeptide, as it has been previously reported that the secondary structure content of CaM (and hence, its far-UV CD spectrum) was not significantly affected upon binding to its targets (*37-39*). However, it cannot be excluded that secondary structural changes also occurred in CaM upon binding to AC.

Previous biochemical and structural studies have shown that the sequence located around tryptophan 242 (W242) represents a major CaM-binding determinant of AC, and that it adopts an amphiphilic helical structure (H helix according to Guo *et al*. (*11*)) typical of many CaM-binding sites. We hypothesized that this segment might undergo a transition from random coil to helical conformation upon association with CaM. We examined therefore potential CaM-induced conformational changes in a synthetic peptide of 22 amino acids residues ($P_{233-254}$) corresponding to the H helix sequence (from residues L233 to G254 in native numbering of CyaA). Intrinsic fluorescence of the single tryptophan residue W242 was used to demonstrate that peptide $P_{233-254}$ bound to CaM (which has no Tryptophan residue) in a calcium-dependent manner, in agreement with previous results (*17*). While the free peptide exhibited a maximum emission wavelength (λ_{max}) at 357 nm, the addition of saturating amounts of CaM resulted in a blue-shift (λ_{max}: 340 nm) and an increase in the fluorescence intensity (inset of figure 2A), suggesting that the W242 moved from a solvent-exposed environment toward a more apolar one. The increase in fluorescence emission at 320 nm was used to monitor binding of peptide $P_{233-254}$ to CaM. These titration experiments (figure 2A) indicated that at concentrations above 1 μM of CaM, the peptide (1 μM) was almost totally bound to CaM. The CaM/peptide interaction was then examined by CD spectroscopy. The far-UV CD spectrum of the free peptide showed a strong negative band at 202 nm, characteristic of extended conformations, while the spectrum of the CaM/peptide complex at same concentration (10 μM) revealed a high helical content (figure 2B). The difference spectrum corresponding to the experimental

spectrum of the $P_{233-254}$/CaM complex minus the sum of the individual $P_{233-254}$ and CaM spectra clearly showed a gain in α-helix structures (inset of figure 2B) upon association. Hence, these data suggest that upon binding to CaM, the $P_{233-254}$ peptide undergoes a transition from a random coil toward a helical-rich conformation.

Near-UV CD spectroscopy was used to characterize the tertiary structure content of AC, CaM and the AC/CaM complex (figure 3A and B). The near-UV CD spectrum of CaM showed two relatively intense negative peaks near 262 and 268 nm arising from phenylalanine residues and a weak negative signal from 270 to 290 nm from tyrosine residues (figure 3A). The near-UV CD spectrum of AC exhibited a large negative band encompassing the aromatic region (figure 3A). The two negative peaks at 262 nm and 269 nm could be assigned to phenylalanine residues, whereas the strong negative band between 270 and 280 nm arose from tyrosine and/or tryptophan residues constrained in chiral environments. It is noteworthy that the L_b band of the 2 tryptophans of AC did not show any chiral activity around 292 nm.

To monitor precisely the changes induced upon association of AC with CaM we used a tandem cuvette in which the two proteins were placed into separated chambers. A spectrum of the separated proteins was first recorded (figure 3B) and then the two proteins were mixed (by inverting the cuvette) before recording a spectrum of the complex. As shown in figure 3B, a slight increase of the dichroic signal from 270 to 285 nm and a significant change around 290 nm, were observed as a result of the interaction between the two proteins. The ellipticity of AC dominates the near-UV CD spectrum because CaM had only minor contributions in this spectral region. Importantly, the appearance of a positive L_b band at 295 nm in the mixed sample could be assigned to the immobilization of the tryptophan residues of AC upon formation of the AC/CaM complex.

The association between CaM and the $P_{233-254}$ peptide was also examined by near-UV CD. As shown in figure 3C, the free peptide showed negligible CD intensities in the near-UV range, as expected for a flexible peptide with its unique aromatic residue (W242) exposed to the solvent. CaM and the peptide were then loaded separately in the tandem cuvette and near-UV CD spectra were recorded before and after mixing. The spectrum of peptide and CaM, in separated compartments of the tandem cuvette, was similar to that of CaM alone (figure 3C), whereas upon mixing of both proteins, a positive band appeared in the tryptophan L_b region (figure 3C). It is noteworthy that this band was very similar to that observed in the spectrum of the AC/CaM complex, suggesting that the dichroic signal at 295 nm arose mainly from the W242 residue of AC.

All together, the CD data suggest that the sequence situated around W242 may adopt an extended conformation in the isolated catalytic domain. CaM-binding could then induce the formation of an α-helix in this region of AC and constrain residue W242 in a chiral environment.

Conformational studies of AC in solution followed by NMR spectroscopy

The 1D spectrum of CaM (figure 4) was characteristic of a structured protein with secondary and tertiary structures: it showed very good dispersion of signals in the aromatic (6-8 ppm) and aliphatic (0-6 ppm) regions, as well as upfield-shifted signals in the methyl region (≤ 0.8 ppm). The existence of some downfield-shifted signals in the Hα region (≥ 5.0 ppm) indicated that the protein contained few residues implicated in β-sheet structures. Conversely, the existence of many upfield-shifted signals with respect to their corresponding random coil values, showed that the protein was rich in α-helical structures. The 1D spectrum of AC also

showed well-spread resonances revealing that the protein was folded (figure 4). Compared to

the spectrum of CaM (17 kDa), the spectrum of AC (42 kDa) displayed very broad lines as

would be expected for a compact protein larger in size. The line width, which depends on the

tumbling rate of a molecule and on its internal dynamics, seemed rather homogeneous in each

region of the spectrum, which suggested that AC did not present large disordered regions. The

Hα region of the AC spectrum showed many downfield-shifted and upfield-shifted

resonances relative to their random coil values, indicative of extensive β-sheet and α-helical

structures, respectively.

The spectrum of the 1:1 (mol/mol) AC:CaM mixture showed broader lines than the AC or

CaM spectra, which indicated that the proteins giving rise to these signals were of higher

molecular weight than AC and CaM, and hence that a complex was formed. Using

apodization functions for Fourier transform to preferentially observe slowly relaxing signals

(narrow lines), we could not detect the spectrum of free CaM. Hence, no significant amount

of free CaM was present in the complex mixture, which indicated that the stoechiometry of

the interaction was 1:1.

The compactness of AC, CaM and of the AC/CaM complex was further analyzed using

saturation transfer experiments (inset of figure 4). The aromatic region of the 1D spectrum of

each sample was saturated by a train of selective 90° pulses, and the intensity of the methyl

region was followed as a function of the saturation time. The high values of the steady state

nOe or transferred saturation (plateau value) obtained for CaM, AC and AC/CaM indicated

that the aromatic residues were in close contact with aliphatic protons, and hence that the

probed molecular species were compact. The magnitude of the steady state nOe depends on

the density of the proton network (compactness) but also on the tumbling rate of a molecule

and hence on it's size. Thus, that the AC/CaM (0.45 ± 0.01) mixture showed a higher steady state nOe than AC (0.39 ± 0.01) and CaM (0.16 ± 0.01), also indicated that the complex was formed.

Hydrodynamic properties of AC/CaM in solution

The hydrodynamic properties (sedimentation coefficient, partial specific volume, molecular mass, hydrodynamic radius, shape and hydration) of AC, CaM and AC/CaM samples were analyzed by combining analytical ultracentrifugation (AUC) and size exclusion chromatography coupled on-line to a Triple Detector Array (SEC-TDA). As shown in figure 5 and table 2, the molecular masses of AC and CaM determined by SEC-TDA (43.8 ± 0.2 kDa for AC and 17.2 ± 0.2 kDa for CaM) corresponded to that expected for the monomeric state of these proteins. The pressure imbalances generated by both proteins and measured by the differential pressure transducers (figure 5C) allowed calculation of an intrinsic viscosity of 5.2 ± 0.1 mL/g for AC and 4.9 ± 0.1 mL/g for CaM (table 2).

The AC/CaM sample was eluted as a major peak (> 90 % of the total intensity) with a molecular mass expected for the AC/CaM complex in a 1:1 stoichiometry (figure 5 and table 2). An intrinsic viscosity of 5 ± 0.1 mL/g was calculated for this AC/CaM complex. A minor peak eluting at a retention volume of 14 mL was detected but the amount was too low to accurately determine the hydrodynamic properties of the species giving rise to this peak. Additional hydrodynamic parameters, listed in table 2, were determined by analytical ultracentrifugation (AUC) (figure 6). In agreement with SEC-TDA, a small amount (less than 15 %) of a higher molecular weight species was observed in the AC/CaM sample in sedimentation velocity experiments (this species was only detected upon data analysis with a low level of confidence - 0.55 instead of 0.95- and because of its low abundance, it could not

be further characterized). From the sedimentation coefficient (S), we determined a hydrodynamic radius (R_H) of 2.3 ± 0.1 nm for CaM, 3.3 ± 0.3 nm for AC, and 3.3 ± 0.3 nm for the complex. These values indicated that a strong compaction occurred upon complex formation as a R_H of at least 3.7 nm would be expected upon addition of the hydrodynamic volumes of the separated proteins. It is noteworthy that quasi-elastic light scattering (QELS) analysis of the same samples gave very similar R_H values (data not shown).

From the hydrodynamic parameters measured by TDA and AUC, we ascribed the respective contributions of hydration and shape factor to the intrinsic viscosity values (*8*). We first extracted the viscosity increment (ν) of the three studied species (table 2 and Experimental Section for details). The viscosity increment is a hydrodynamic function related to the axial ratio (a/b) of the semi-axes a and b of an ellipsoid of revolution (*40*). The viscosity increment of CaM corresponded to that of an elongated shape (a/b ≈ 2), in good agreement with the known 3D structure that consists of two globular domains connected by an elongated and flexible linker (*32*). In contrast, the isolated AC domain exhibited a viscosity increment of 2.5 that corresponds to an axial ratio a/b of 1 (a=b=R_H) (*40*). This result suggests that AC adopted a spherical conformation. Interestingly, the value of the viscosity increment of the AC/CaM complex indicated that its shape diverged significantly from that of a sphere. Indeed, with an axial ratio of ~ 2.7 (table 2), the complex adopted an elongated shape in good agreement with that found in the X-ray structure (*11*). Finally, we determined the hydration parameter (δ_{IV}) using the intrinsic viscosity relation (see Experimental Section). This parameter corresponds to the water molecules bound to the protein as well as to the water molecules dragged by the diffusion of the protein and/or influenced by being in the vicinity of the protein. The isolated CaM and AC displayed a hydration of 1 ± 0.1 g.g^{-1} and 1.5 ± 0.1 g.g^{-1}, respectively.

Interestingly, the hydration decreased markedly to 0.7 ± 0.1 g.g^{-1} upon complex formation

(table 2). These data indicate that both AC and CaM underwent dehydration upon interaction.

Discussion

In this report, we have characterized the conformational and hydrodynamic changes of the

CyaA catalytic domain (AC) triggered by CaM binding in an attempt to obtain biophysical

insights into the molecular mechanisms underlying the activation of the AC enzymatic

activity.

The secondary and tertiary structure changes of the polypeptides were first characterized by

CD and NMR spectroscopies. We showed that the secondary structure of AC is an

α/β mixture, without large disordered regions. A prominent finding from CD experiments

was that only minor modifications of the secondary structure content of the AC and CaM

polypeptides occurred upon their association. Nevertheless, comparison of far-UV CD spectra

indicated that CaM association with AC triggered a small but detectable increment of the

overall α-helical structure content of these proteins. We calculated that about 4 % of total

secondary structure, corresponding to about 20 residues out of a total of 534, changed from

random coil conformations to α-helical structures upon complex formation. Although the

polypeptide region(s) involved in this transition cannot be formally localized, we

hypothesized that this structural change occurred in part within the H helix of AC (according

to the nomenclature of Guo *et al*. (*11*); see figure 7), which constitutes the main CaM-binding

site. In agreement with this hypothesis, far-UV CD spectroscopy indicated that a synthetic

peptide, P$_{233-254}$, corresponding to H helix (from residues L233 to G254), adopted random coil

conformations in the absence of CaM but acquired helical structures upon binding to CaM, as

it has been observed for many other CaM-binding peptides derived from different CaM targets.

Near-UV CD and fluorescence spectroscopies analysis confirmed that whereas in the free peptide $P_{233-254}$, the tryptophan 242 (W242) was exposed to solvent and highly mobile, it became constrained upon CaM-binding, as revealed by the dichroic signal increase at 295 nm and a large blue-shift in intrinsic fluorescence. Interestingly, very similar changes in near-UV CD and fluorescence signals (not shown and (*41*) for fluorescence data) were observed with the AC domain as it bound CaM, suggesting that the CaM-induced local structural rearrangement may be similar in both cases. These data are in good agreement with previous results (*42, 43*), which used time-resolved fluorescence spectroscopy to probe the dynamics of W242. These authors reported that the AC region surrounding this residue was highly dynamic showing nanosecond flexibility in the CaM-free form, and that binding of the activator greatly decreased the local dynamics. It is noteworthy that in anthrax EF, the equivalent H helix is also partly disordered in the CaM-free structure.

All together our data are consistent with a model in which the region around W242 may preferentially adopt an extended conformation in the absence of CaM with the tryptophan being highly mobile and solvent-exposed. Upon association with CaM, this segment would be stabilized in a helical conformation (H helix) and the W242 would become immobilized in a hydrophobic pocket of CaM_{C-ter} as seen in the crystal structure (*11*).

While CaM-binding elicited only minor changes in the secondary and tertiary structure of AC, it had much more pronounced effect of the hydrodynamic properties of the AC protein. Using analytical ultracentrifugation and size exclusion chromatography (SEC) combined with static

light scattering and viscosity measurements, we showed that the isolated AC domain was monomeric under native conditions, and adopted a globular conformation with a rather high hydration. Upon complex formation, the hydration δ_{IV} decreased significantly and the shape became much more elongated with an axial ratio of ~ 2.7. This latter value is in good agreement with the one computed from the crystal structure of AC/CaM$_{C\text{-ter}}$, although in this complex the N-terminal half of CaM (CaM$_{N\text{-ter}}$) is absent.

The hydrodynamic properties of AC have also been explored by Gallay *et al*. (*43*), on the basis of fluorescence anisotropy decay measurements. They showed that the average Brownian rotational correlation times of AC differed significantly as a function of the fluorescent probes examined (either AC tryptophans or a fluorescent ATP analog or a covalently attached acrylodan probe). It was suggested that AC in the absence of CaM may adopt an elongated shape (with an axial ratio of about 1.9) that would become more elongated (axial ratio of 2.4) upon CaM binding. Although our results agree with a CaM-induced elongation of the AC molecule, they are at variance regarding the overall shape of the free AC protein, as we found that AC is rather globular in the absence of CaM. Indeed, the viscosity increment of 2.5 calculated for the free AC in solution corresponds to an axial ratio a/b of 1 (a=b=R$_H$), which is indicative of a nearly spherical conformation. The discrepancy regarding the shape of AC may be related to the different experimental approaches used. Indeed, Gallay and colleagues estimated the dynamics of the whole protein by extrapolation of time-resolved fluorescence anisotropy decays of small probes. Yet, these values depend not only on the overall protein hydrodynamics, but also on the probe flexibility. In the present study, the hydrodynamic properties of the proteins were characterized by AUC, SEC-TDA and DLS. These latter biophysical approaches provide hydrodynamic parameters based directly on the behavior of the corresponding molecules and therefore should be considered as more reliable.

The observation that AC adopts a globular conformation in the absence of CaM has direct implications onto the possible conformational changes elicited by CaM-binding. In the crystal structure, the AC/CaM complex appears as an extended rod of about 10 nm long and about 4 nm in diameter (figure 7). One tip of this rod is made by the H helix, bound to CaM_{C-ter}, together with the two preceding short helices F and G at the C-terminus of the T25 region. The H helix is aligned with the main axis of the rod and points out, contributing to about a third of the AC overall length. Based on our data, we can hypothesize that in the absence of CaM, this helical tip as well as the T18 region (in dark blue in figure 7) fold back onto the core of the T25 region of the catalytic domain (figure 7). This structural organization may be associated with a partially unfolded H helix as suggested from our CD data discussed above. Such a reorientation of the F, G and H helices and the rest of the T18 region relative to the catalytic core would significantly shorten the long axis of the molecule, hence giving rise to a much more globular conformation in agreement with our hydrodynamic measurements.

It is interesting to note that the corresponding F, G and H helices of the anthrax EF toxin -the so-called switch A according to Drum *et al*. (*15*)- also undergo a significant conformational rearrangement between the CaM-free and CaM-bound forms, in a fairly similar way to the one suggested above for AC. In the CaM-bound form, the H helix of *B*. *anthracis* EF is also roughly aligned with the main axis of the catalytic core (domains C_A and C_B). In the absence of CaM, the H helix is rotated of about 50 ° relative to the main axis to dock onto the C-terminal helical domain, which is the main CaM-binding site of EF (*15*). It is noteworthy that, as in AC an equivalent C-terminal helical domain is absent, the corresponding H helix would have enough space to rotate up to 90 ° in the CaM-free conformation and dock onto the side of the C_A domain of the catalytic core.

CaM establishes numerous contact with the T18 moiety of AC, predominantly with the H helix, but also with the C-terminal helices J and J' ("C-tail" according to Guo *et al*. (*11*)) and thus may directly contribute to lock the T18 region into a stable and active conformation. In the absence of this activator, the T18 polypeptide might be more flexible and hydrated as suggested by our results. Our present data actually support the view that the secondary structure content of the T18 fragment is not dramatically altered in the CaM-free AC, as evidenced from the global conservation of the secondary structures (CD), the absence of large disordered regions (NMR) and the overall globular shape (hydrodynamic studies) of the molecule. The reorganization of the helical tip (i.e. F, G and H helices) in the CaM-free AC may be accompanied by some repositioning of the T18 polypeptide, thus disrupting the local topological arrangement of the CR3 region of the catalytic site and consequently altering the enzymatic activity. A higher dynamics of the whole T18 polypeptide and especially of the CR3 region may also contribute to the dramatic reduction of the catalytic efficiency of the AC enzyme in the absence of the activator. This model could explain that AC retains a weak but detectable enzymatic activity in the absence of CaM, at variance with EF, which appears to be locked in a totally inactive state in the absence of the activator.

In conclusion, the results presented here shed new light on the molecular shape of the catalytic domain of CyaA and on the structural rearrangements elicited by CaM-binding. Our data indicate that although CaM binding triggers only limited modifications in the secondary and tertiary structures of AC, it induces a significant elongation, dehydration and compaction of the protein. We propose that these conformational changes stabilize the enzymatically active form of AC by remodeling the catalytic site, in a very similar process to that found in EF. This would suggest that the *B. pertussis* and *B. anthracis* adenylate cyclase toxins share a common mechanism of activation although their primary sequence and structural basis for

interacting with their common CaM activator have largely diverged.

References

1.   Ladant, D., and Ullmann, A. (1999) Bordatella pertussis adenylate cyclase: a toxin with multiple talents, *Trends Microbiol 7*, 172-176.

2.   Vojtova, J., Kamanova, J., and Sebo, P. (2006) Bordetella adenylate cyclase toxin: a swift saboteur of host defense, *Curr Opin Microbiol 9*, 69-75.

3.   Harvill, E. T., Cotter, P. A., Yuk, M. H., and Miller, J. F. (1999) Probing the function of Bordetella bronchiseptica adenylate cyclase toxin by manipulating host immunity, *Infect Immun 67*, 1493-1500.

4.   Perkins, D. J., Gray, M. C., Hewlett, E. L., and Vogel, S. N. (2007) Bordetella pertussis adenylate cyclase toxin (ACT) induces cyclooxygenase-2 (COX-2) in murine macrophages and is facilitated by ACT interaction with CD11b/CD18 (Mac-1), *Mol Microbiol 66*, 1003-1015.

5.   Cheung, G. Y., Dickinson, P., Sing, G., Craigon, M., Ghazal, P., Parton, R., and Coote, J. G. (2008) Transcriptional responses of murine macrophages to the adenylate cyclase toxin of Bordetella pertussis, *Microb Pathog 44*, 61-70.

6.   Rose, T., Sebo, P., Bellalou, J., and Ladant, D. (1995) Interaction of calcium with Bordetella pertussis adenylate cyclase toxin. Characterization of multiple calcium-binding sites and calcium-induced conformational changes, *The Journal of biological chemistry 270*, 26370-26376.

7.   Bauche, C., Chenal, A., Knapp, O., Bodenreider, C., Benz, R., Chaffotte, A., and Ladant, D. (2006) Structural and functional characterization of an essential RTX subdomain of Bordetella pertussis adenylate cyclase toxin, *The Journal of biological chemistry 281*, 16914-16926.

8.   Chenal, A., Guijarro, J. I., Raynal, B., Delepierre, M., and Ladant, D. (2009) RTX calcium binding motifs are intrinsically disordered in the absence of calcium: implication for protein secretion, *The Journal of biological chemistry 284*, 1781-1789.

9.   Danchin, A. (1993) Phylogeny of adenylyl cyclases, *Adv Second Messenger Phosphoprotein Res 27*, 109-162.

10.   Shen, Y., Zhukovskaya, N. L., Guo, Q., Florian, J., and Tang, W. J. (2005) Calcium-independent calmodulin binding and two-metal-ion catalytic mechanism of anthrax edema factor, *Embo J 24*, 929-941.

11.   Guo, Q., Shen, Y., Lee, Y. S., Gibbs, C. S., Mrksich, M., and Tang, W. J. (2005) Structural basis for the interaction of Bordetella pertussis adenylyl cyclase toxin with calmodulin, *Embo J 24*, 3190-3201.

12.   Glaser, P., Elmaoglou-Lazaridou, A., Krin, E., Ladant, D., Barzu, O., and Danchin, A. (1989) Identification of residues essential for catalysis and binding of calmodulin in Bordetella pertussis adenylate cyclase by site-directed mutagenesis, *Embo J 8*, 967-972.

13.   Glaser, P., Munier, H., Gilles, A. M., Krin, E., Porumb, T., Barzu, O., Sarfati, R., Pellecuer, C., and Danchin, A. (1991) Functional consequences of single amino acid

substitutions in calmodulin-activated adenylate cyclase of Bordetella pertussis, *Embo J 10*, 1683-1688.

14. Munier, H., Bouhss, A., Krin, E., Danchin, A., Gilles, A. M., Glaser, P., and Barzu, O. (1992) The role of histidine 63 in the catalytic mechanism of Bordetella pertussis adenylate cyclase, *The Journal of biological chemistry 267*, 9816-9820.

15. Drum, C. L., Yan, S. Z., Bard, J., Shen, Y. Q., Lu, D., Soelaiman, S., Grabarek, Z., Bohm, A., and Tang, W. J. (2002) Structural basis for the activation of anthrax adenylyl cyclase exotoxin by calmodulin, *Nature 415*, 396-402.

16. Ladant, D. (1988) Interaction of Bordetella pertussis adenylate cyclase with calmodulin. Identification of two separated calmodulin-binding domains, *The Journal of biological chemistry 263*, 2612-2618.

17. Ladant, D., Michelson, S., Sarfati, R., Gilles, A. M., Predeleanu, R., and Barzu, O. (1989) Characterization of the calmodulin-binding and of the catalytic domains of Bordetella pertussis adenylate cyclase, *The Journal of biological chemistry 264*, 4015-4020.

18. Munier, H., Bouhss, A., Gilles, A. M., Krin, E., Glaser, P., Danchin, A., and Barzu, O. (1993) Structural flexibility of the calmodulin-binding locus in Bordetella pertussis adenylate cyclase. Reconstitution of catalytically active species from fragments or inactive forms of the enzyme, *European journal of biochemistry / FEBS 217*, 581-586.

19. Bouhss, A., Krin, E., Munier, H., Gilles, A. M., Danchin, A., Glaser, P., and Barzu, O. (1993) Cooperative phenomena in binding and activation of Bordetella pertussis adenylate cyclase by calmodulin, *The Journal of biological chemistry 268*, 1690-1694.

20. Guo, Q., Jureller, J. E., Warren, J. T., Solomaha, E., Florian, J., and Tang, W. J. (2008) Protein-protein docking and analysis reveal that two homologous bacterial

adenylyl cyclase toxins interact with calmodulin differently, *The Journal of biological chemistry 283*, 23836-23845.

21.   Vougier, S., Mary, J., Dautin, N., Vinh, J., Friguet, B., and Ladant, D. (2004) Essential role of methionine residues in calmodulin binding to Bordetella pertussis adenylate cyclase, as probed by selective oxidation and repair by the peptide methionine sulfoxide reductases, *The Journal of biological chemistry 279*, 30210-30218.

22.   Lees, J. G., Miles, A. J., Wien, F., and Wallace, B. A. (2006) A reference database for circular dichroism spectroscopy covering fold and secondary structure space, *Bioinformatics (Oxford, England) 22*, 1955-1962.

23.   Lobley, A., Whitmore, L., and Wallace, B. A. (2002) DICHROWEB: an interactive website for the analysis of protein secondary structure from circular dichroism spectra, *Bioinformatics (Oxford, England) 18*, 211-212.

24.   Whitmore, L., and Wallace, B. A. (2004) DICHROWEB, an online server for protein secondary structure analyses from circular dichroism spectroscopic data, *Nucleic acids research 32*, W668-673.

25.   Compton, L. A., and Johnson, W. C., Jr. (1986) Analysis of protein circular dichroism spectra for secondary structure using a simple matrix multiplication, *Analytical biochemistry 155*, 155-167.

26.   Sreerama, N., and Woody, R. W. (2000) Estimation of protein secondary structure from circular dichroism spectra: comparison of CONTIN, SELCON, and CDSSTR methods with an expanded reference set, *Analytical biochemistry 287*, 252-260.

27.   Manavalan, P., and Johnson, W. C., Jr. (1987) Variable selection method improves the prediction of protein secondary structure from circular dichroism spectra, *Analytical biochemistry 167*, 76-85.

28.   Cao, W., and Demeler, B. (2005) Modeling analytical ultracentrifugation experiments with an adaptive space-time finite element solution of the Lamm equation, *Biophys J 89*, 1589-1602.

29.   Schuck, P. (2000) Size-distribution analysis of macromolecules by sedimentation velocity ultracentrifugation and lamm equation modeling, *Biophys J 78*, 1606-1619.

30.   Schuck, P. (2003) On the analysis of protein self-association by sedimentation velocity analytical ultracentrifugation, *Analytical biochemistry 320*, 104-124.

31.   Bourdeau, R. W., Malito, E., Chenal, A., Bishop, B. L., Musch, M. W., Villereal, M. L., Chang, E. B., Mosser, E. M., Rest, R. F., and Tang, W. J. (2009) Cellular Functions and X-ray Structure of Anthrolysin O, a Cholesterol-dependent Cytolysin Secreted by Bacillus anthracis, *The Journal of biological chemistry 284*, 14645-14656.

32.   Barbato, G., Ikura, M., Kay, L. E., Pastor, R. W., and Bax, A. (1992) Backbone dynamics of calmodulin studied by 15N relaxation using inverse detected two-dimensional NMR spectroscopy: the central helix is flexible, *Biochemistry 31*, 5269-5278.

33.   Sreerama, N., Manning, M. C., Powers, M. E., Zhang, J. X., Goldenberg, D. P., and Woody, R. W. (1999) Tyrosine, phenylalanine, and disulfide contributions to the circular dichroism of proteins: circular dichroism spectra of wild-type and mutant bovine pancreatic trypsin inhibitor, *Biochemistry 38*, 10814-10822.

34.   Freskgard, P. O., Martensson, L. G., Jonasson, P., Jonsson, B. H., and Carlsson, U. (1994) Assignment of the contribution of the tryptophan residues to the circular dichroism spectrum of human carbonic anhydrase II, *Biochemistry 33*, 14281-14288.

35.   Tavallaie, M., Chenal, A., Gillet, D., Pereira, Y., Manich, M., Gibert, M., Raffestin, S., Popoff, M. R., and Marvaud, J. C. (2004) Interaction between the two subdomains

of the C-terminal part of the botulinum neurotoxin A is essential for the generation of protective antibodies, *FEBS Lett 572*, 299-306.

36.　(1996) *Circular Dichroism and the Conformational Analysis of Biomolecules*, (Fasman, G.D., ed.) Plenum Press, New York and London.

37.　Ikura, M., Clore, G. M., Gronenborn, A. M., Zhu, G., Klee, C. B., and Bax, A. (1992) Solution structure of a calmodulin-target peptide complex by multidimensional NMR, *Science 256*, 632-638.

38.　Meador, W. E., Means, A. R., and Quiocho, F. A. (1992) Target enzyme recognition by calmodulin: 2.4 A structure of a calmodulin-peptide complex, *Science 257*, 1251-1255.

39.　Meador, W. E., Means, A. R., and Quiocho, F. A. (1993) Modulation of calmodulin plasticity in molecular recognition on the basis of x-ray structures, *Science 262*, 1718-1721.

40.　Harding, S. E., and Colfen, H. (1995) Inversion formulae for ellipsoid of revolution macromolecular shape functions, *Analytical biochemistry 228*, 131-142.

41.　Gilles, A. M., Munier, H., Rose, T., Glaser, P., Krin, E., Danchin, A., Pellecuer, C., and Barzu, O. (1990) Intrinsic fluorescence of a truncated Bordetella pertussis adenylate cyclase expressed in Escherichia coli, *Biochemistry 29*, 8126-8130.

42.　Bouhss, A., Vincent, M., Munier, H., Gilles, A. M., Takahashi, M., Barzu, O., Danchin, A., and Gallay, J. (1996) Conformational transitions within the calmodulin-binding site of Bordetella pertussis adenylate cyclase studied by time-resolved fluorescence of Trp242 and circular dichroism, *European journal of biochemistry / FEBS 237*, 619-628.

43.　Gallay, J., Vincent, M., Li de la Sierra, I. M., Munier-Lehmann, H., Renouard, M., Sakamoto, H., Barzu, O., and Gilles, A. M. (2004) Insight into the activation

mechanism of Bordetella pertussis adenylate cyclase by calmodulin using

fluorescence spectroscopy, *European journal of biochemistry / FEBS 271*, 821-833.

Table 1: Secondary structure of CaM, AC and AC/CaM

Secondary structure composition	CaM[a]	AC[a]	AC/CaM[a]	AC + CaM[b]
α-Helix	50	24	35	31
β-Sheet	14	19	13	18
Turns	14	17	18	16
Random coil	21	40	34	35
Root mean square error	0.012	0.022	0.034	

Deconvolution of the far-UV CD spectra was performed using DICHROWEB (*23*).
The deconvolution results shown here are those provided by the CDSSTR software.
[a] from experimental data
[b] theoretical sum of the spectra of AC and CaM

Table 2: Hydrodynamic parameters of CaM, AC and AC/CaM

Parameters	CaM	AC	AC-CaM
Retention volume[a] (mL)	18.5 ± 0.1	17.2 ± 0.1	16.0 ± 0.1
Molecular mass[a] (kDa)	17.3 ± 0.2	43.8 ± 0.2	58.4 ± 0.2
Intrinsic viscosity[a] (mL/g)	4.9 ± 0.1	5.2 ± 0.1	5.0 ± 0.1
Partial specific volume[b] $\bar{v}$ (mL/g)	0.740 ± 0.001	0.736 ± 0.001	0.745 ± 0.001
Sedimentation coefficient[b] (S)	2.0 ± 0.1	3.3 ± 0.2	4.4 ± 0.4
R_0 anhydrous[c] (nm)	1.7	2.3	2.6
R_H[b] (nm)	2.3 ± 0.1	3.3 ± 0.3	3.3 ± 0.3
Frictional ratio[b] (f/fo)	1.32 ± 0.07	1.44 ± 0.09	1.26 ± 0.11
Viscosity increment[d]	2.9 ± 0.2	2.4 ± 0.2	3.4 ± 0.3
a/b[e]	2.0 ± 0.4	1	2.7 ± 0.3
Hydration[d] δ_{IV} (g/g)	1.0 ± 0.1	1.5 ± 0.1	0.7 ± 0.1
Computed hydration (g/g)[f]	0.48	0.41	0.43

[a] Experimental data from TDA

[b] Experimental data from AUC

[c] Hydrodynamic radius of an anhydrous and spherical molecule with equivalent M and $\bar{v}$

[d] The viscosity increment and hydration were calculated as described in Experimental Section

[e] Assuming a prolate shape

[f] Computed using SEDNTERP.

Figure Legends

Figure 1: Far-UV CD spectra of AC, CaM and AC/CaM complex. (**A**) Far-UV CD spectra of AC (25 μM; dotted line), CaM (25 μM; dashed line) and the AC/CaM complex (25 μM of both proteins; continuous line). (**B**) The sum of the spectra of the two isolated components is reported (thin line) for comparison with the AC/CaM experimental spectrum (bold line). Inset: calculated difference between the spectrum of the mixture of the two components and the sum of the spectra of the unmixed components. Experimental conditions: buffer A at 25 °C supplemented with 0.2 mM $CaCl_2$.

Figure 2: Fluorescence and far-UV CD spectra of the peptide $P_{233-254}$ in the presence and absence of CaM. (**A**) Fluorescence intensity at 320 nm (Ex.: 290 nm) of 1 μM peptide $P_{233-254}$ in the presence of increasing amount of CaM (from 0 to 10 μM). Spectra were averaged (three replicates) and the contribution of the buffer was subtracted. Inset, tryptophan intrinsic fluorescence spectra of the peptide $P_{233-254}$ (1 μM) in the absence (continuous line) or in the presence of CaM (dashed line). (**B**) Far-UV CD spectra of the free peptide $P_{233-254}$ (90 μM; dotted line), and the $P_{233-254}$/CaM complex (25 μM of both components; bold line). The sum of the spectra of the two isolated components (at same concentration of 25 μM) is also reported for comparison (thin line). Inset: calculated difference between the spectrum of the mixture of the two components and the sum of the spectra of the unmixed components. In (**B**), scales have been adjusted in order to show the difference between spectra. Experimental conditions: buffer A, 0.2 mM $CaCl_2$ at 25 °C.

Figure 3: Near-UV CD spectra of AC, CaM and AC/CaM complex, as well as of peptide $P_{233-254}$ and of the peptide/CaM complex. (**A**) Near-UV CD spectra of AC (30 μM; dotted line) and

CaM (30μM; dashed line) (**B**) Near-UV CD spectra of AC and CaM (30 μM each protein) either separated (thin line) or mixed (bold line) in a tandem cuvette. (**C**) Near-UV CD spectra of the free peptide P$_{233\text{-}254}$ (45 μM; dotted line) and of P$_{233\text{-}254}$ and CaM (45 μM and 30 μM, respectively) either separated (thin line) or mixed (bold line) in a tandem cuvette. The arrows highlight the region of the tryptophan Lb band. Experimental conditions: buffer A, 0.2 mM CaCl$_2$ at 25 °C.

Figure 4: NMR one-dimensional proton spectra of CAM (bottom), AC (middle) and a 1:1 AC:CAM mixture (top) acquired at 25 °C in deuterated buffer A. The peaks belonging to residual water and the buffer are indicated with an asterisk. Inset, saturation transfer experiments. The intensity of the nOe between aromatic and aliphatic protons as a function of the saturation time is displayed. The solid line corresponds to the fit of the nOe data to an isolated spin-pair model as indicated in the Experimental section.

Figure 5: Size exclusion chromatography as followed by a triple detector array (Viscotek) of AC (dotted line), CaM (dashed line), and AC/CaM complex (continuous line). (**A**) UV absorption chromatogram. (**B**) Right angle light scattering chromatogram. (**C**) Differential pressure chromatogram. (**D**) Molecular mass (left y axis, bold line) and intrinsic viscosity (right y axis, thin line) are given for each species. Experimental conditions: buffer A, 0.2 mM CaCl$_2$ at 25 °C.

Figure 6: Analytical ultracentrifugation analysis of AC, CaM and AC/CaM complex (17 μM in buffer A). Experimental data (dots) obtained at 276 nm during AC (**A**) and AC/CaM (**C**) sedimentation velocity experiments were fitted with the Lamm equation (lines) and the distribution of the residual values is shown in panel (**B**) and (**D**) respectively. (**E**)

Sedimentation coefficient distribution of AC (dotted line), CaM (dashed line), and AC/CaM complex (continuous line) deduced from the fitted curves. Experimental conditions: buffer A at 25 °C supplemented with 0.2 mM $CaCl_2$.

Figure 7: Three-dimensional structure of AC complexed with the C-terminal domain of CaM. The picture is drawn from pdb file 1YRU (*11*) to highlight the positioning of the helical tip made of F, G and H helices. CaM_{C-ter} is shown in yellow whereas the T25 and T18 AC regions are represented in green and blue, respectively. The side chain of AC W242, buried in a hydrophobic pocket of CaM, is indicated in dark blue.
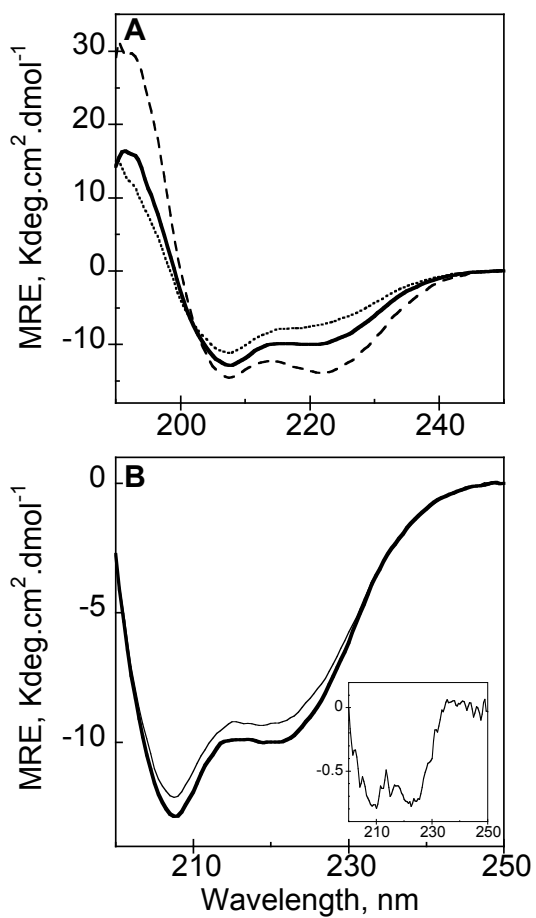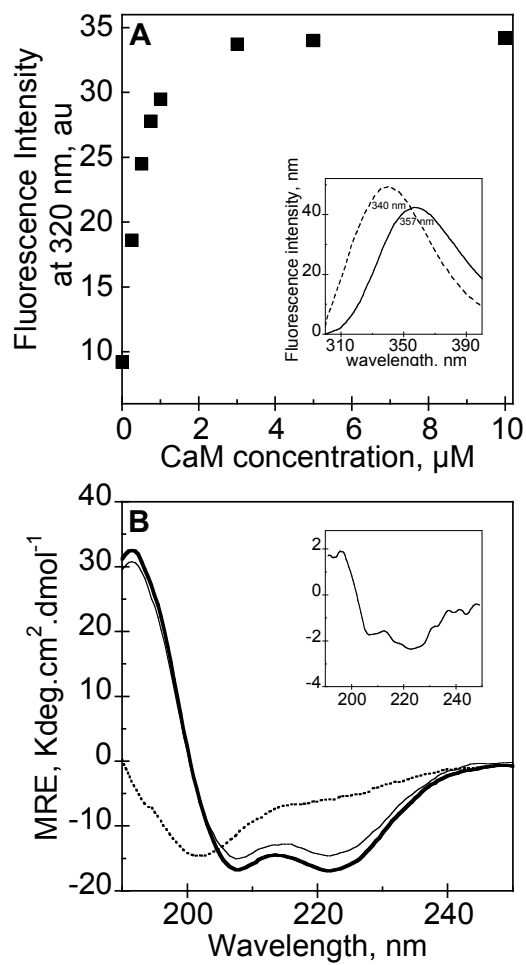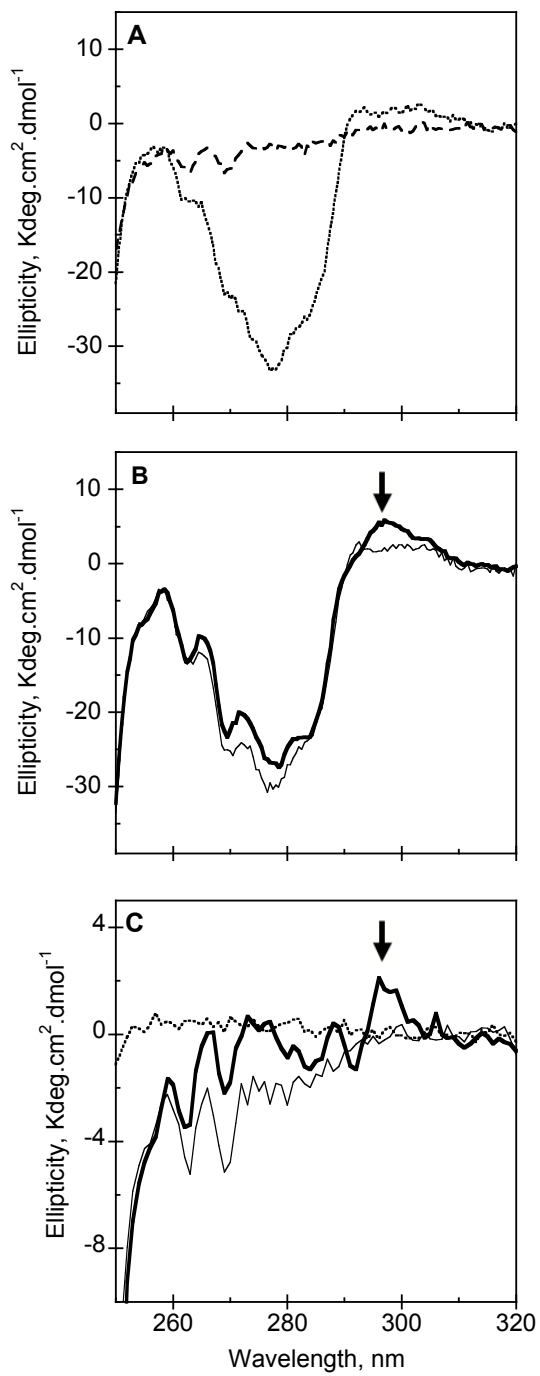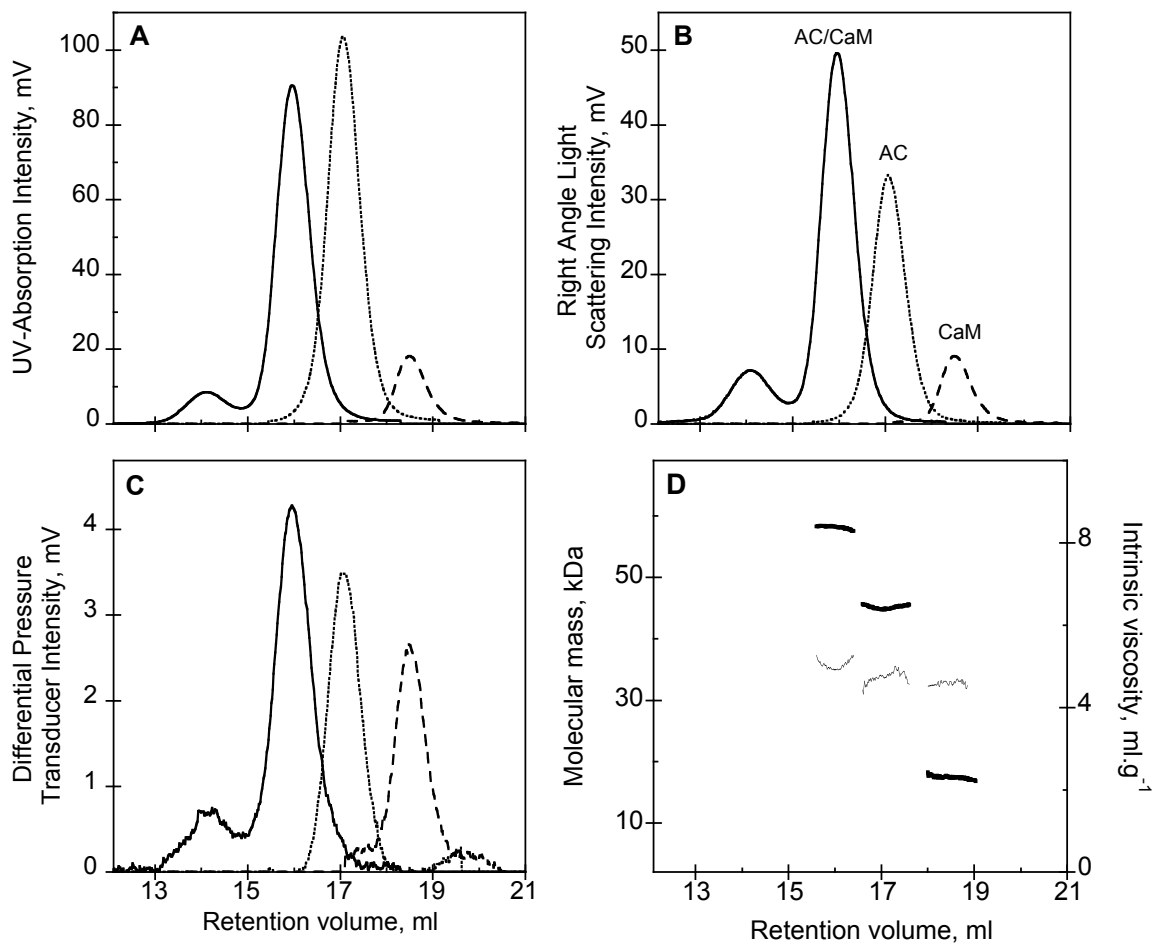
Figure 1

Figure 2

Figure 3
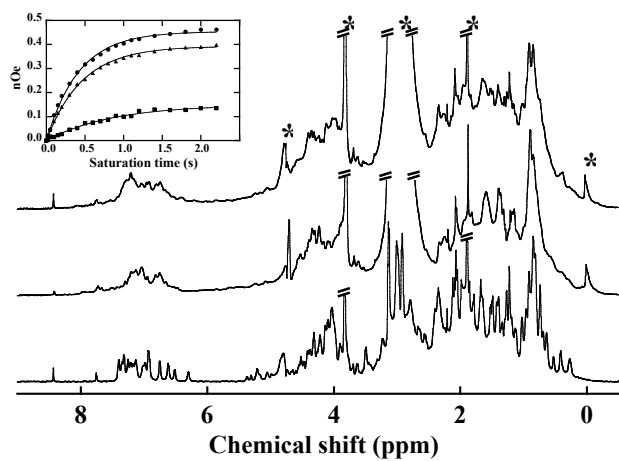
Figure 4

Figure 5
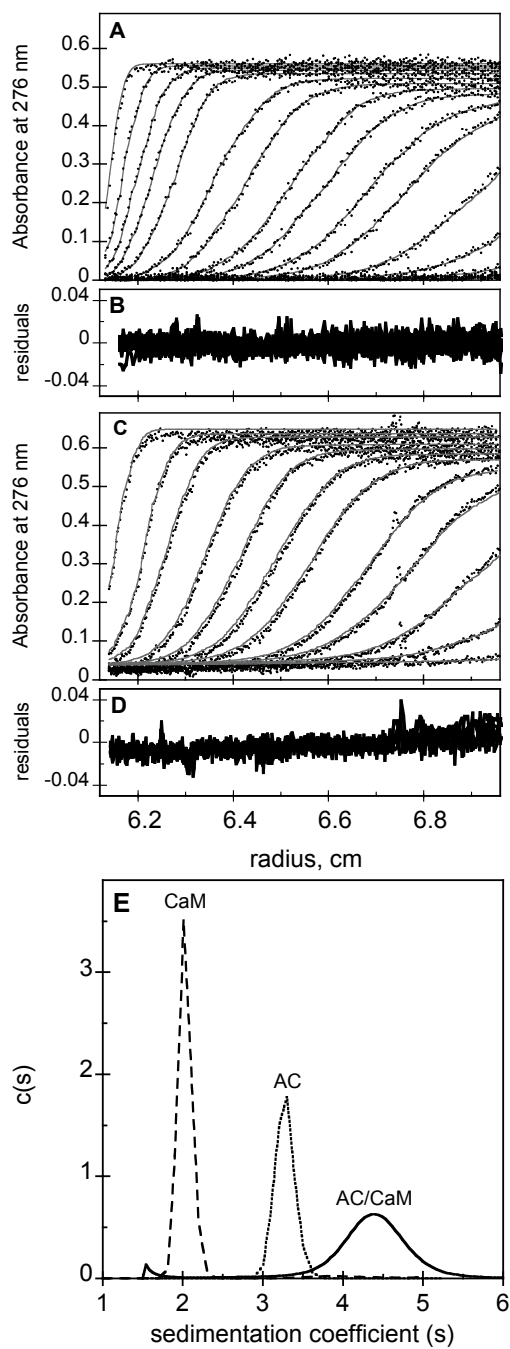
Figure 6
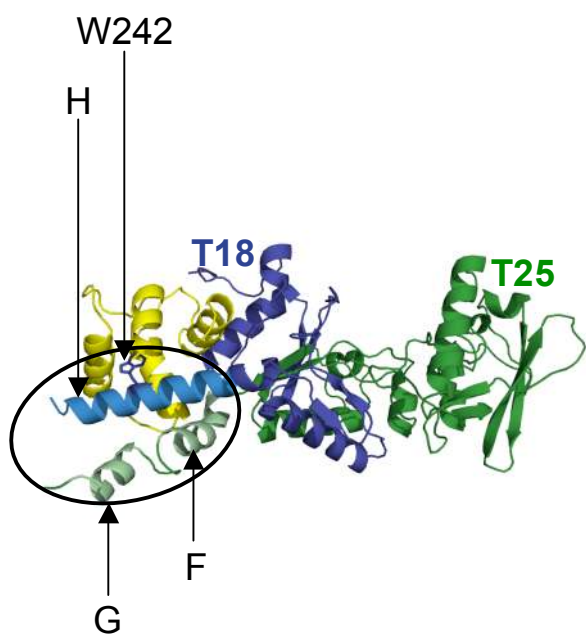
Figure 7

For Table of Contents Use Only

Calmodulin-Induced Conformational and Hydrodynamic Changes of the Catalytic Domain of *Bordetella pertussis* Adenylate Cyclase Toxin †

Johanna C. Karst, Ana Cristina Sotomayor Pérez, J. Iñaki Guijarro, Bertrand Raynal, Alexandre Chenal, and Daniel Ladant